

## 1.5 DISTRIBUTED ACCELERATION SENSING FOR SMALL UAS WIND GUST ESTIMATION

Emily A. Ranquist\* Sean Humbert† and Brian Argrow‡  
University of Colorado Boulder, Boulder, Colorado\*†‡

### 1. INTRODUCTION

Small unmanned aircraft systems (sUAS) are increasingly being used for a variety of applications due to their low cost, ability to fly in dangerous or inaccessible areas, and operational ease. One area in which sUAS are being used extensively is atmospheric research. Examples of current studies in which these aircraft have played a role are tornado and hurricane formation (Avery 2015), lower atmospheric boundary layer characterization (Reuder 2012), dynamic soaring (Quindlen 2013), and urban wind field mapping (Cybyk 2009).

Wind information is a critical aspect of many of these studies and also an important factor in aircraft performance and control. Using sUAS as a means of wind measurement is more advantageous than traditional ground wind sensing, such as from a tower, due to the ability to measure in any flight pattern and at any location, while still being able to capture temporal changes at high sampling rates (Weibel 2015).

However, a few difficulties arise when using sUAS for wind sensing. First, the low payload capacity and small size limit the type and amount of wind sensing equipment that can feasibly be placed on board. Some companies have created micro wind velocity data acquisition systems with lower sizes and weights for use on sUAS (Aeroprobe 2018), but these systems cost thousands of dollars, which is often more expensive than the sUAS airframe itself. Furthermore, commonly used wind velocity sensors such as multi-hole probes and hot-wire anemometers must be calibrated using known wind velocity information (e.g. from a wind tunnel) before they can be used. These sensors do not

measure inertial wind, but rather the wind velocity relative to the aircraft.

An additional difficulty that arises is a lack of control of sUAS in turbulent environments. Small UAS have lower inertia, lower wing loading, smaller masses, and smaller wingspans than their manned counterparts, which results in these aircraft having a harder time maintaining control in windy conditions (Pisano 2009). In the event of complete loss of control, there is a high likelihood of damage to any protruding sensors.

For these reasons, alternative methods of wind measurement have been proposed and studied using smaller and cheaper sensors that are integrated inside the fuselage or flush with the aircraft. Many of these methods have depended on velocity and attitude estimates from the global positioning system (GPS) and inertial measurement unit (IMU). In the presence of strong wind, significant errors are induced in attitude and aircraft velocity measurements from these sensors (Weibel 2015), which suggests that the use of cheap sensors with little or no redundancy comes at the expense of accuracy in wind measurements.

The primary focus of this paper is to propose a method of inertial wind velocity state estimation for a fixed-wing UAS that does not use any air flow probes, but rather utilizes acceleration information from a distributed accelerometer sensor suite. This method eliminates the aforementioned difficulties with current wind measurement methods on sUAS because distributed accelerometers are lightweight, robust, inexpensive, and redundant. Furthermore, distributed accelerometers provide angular acceleration information that can be used to extract components of the wind velocity gradient tensor, which allows for improved resolution of the 3D wind vector estimates. Wind velocity gradient information cannot be obtained with a single IMU nor multi-hole probe.

The wind velocity estimation technique discussed in this paper utilizes a linearized aerodynamic model of the Tempest UAS and the structure of the Dryden Turbulence Model in order to make wind velocity estimates. This estimation technique was compared with and without acceleration feedback in simulation using Simulink

---

*Corresponding author addresses:*

\* Emily Ranquist, Univ. of Colorado Boulder, Dept. of Aerospace Engineering Sciences, Boulder, CO 80301;  
e-mail: [emily.ranquist@colorado.edu](mailto:emily.ranquist@colorado.edu)

† Sean Humbert, Univ. of Colorado Boulder, Dept. of Mechanical Engineering, Boulder, CO 80301;  
email: [sean.humbert@colorado.edu](mailto:sean.humbert@colorado.edu)

‡ Brian Argrow, Univ. of Colorado Boulder, Dept. of Aerospace Engineering Sciences, Boulder, CO 80301;  
email: [brian.argrow@colorado.edu](mailto:brian.argrow@colorado.edu)

and MATLAB. The remainder of this paper will discuss the wind velocity state estimation methodology, the simulation setup, and the results as compared to known simulated wind velocities.

## 2. WIND VELOCITY STATE ESTIMATION

A major advantage of state estimation is the ability to accurately estimate unknown or unmeasurable states of a system despite noisy measurements or errors in the system model. This can be achieved through the use of a state observer, such as a Kalman Filter, which reduces the error between the system model and the known states obtained from sensor measurements. Many of the existing wind velocity estimation studies that have been employed on sUAS have utilized the relationship between wind speed, airspeed, and ground speed (i.e. the wind triangle), which requires an airspeed sensor (Cho 2011, Johansen 2015). As mentioned prior, these sensors can be prohibitive for use on sUAS in terms of cost, size, and weight.

The wind velocity estimation technique described in this study does not require an airspeed sensor, but rather relies on a linearized state space model of the aircraft and wind to perform state estimation through a Kalman Filter. Typical linear state space models are of the form,

$$\dot{\mathbf{x}} = \mathbf{A}\mathbf{x} + \mathbf{B}\mathbf{u} + \mathbf{G}\mathbf{d} \quad (2.1a)$$

$$\mathbf{y} = \mathbf{C}\mathbf{x} + \mathbf{D}\mathbf{u} \quad (2.1b)$$

where  $\mathbf{x}$  represents the state vector comprised of the states of the system (e.g. position, velocity),  $\mathbf{u}$  is the input vector,  $\mathbf{d}$  is a vector that describes a perturbation from an equilibrium condition,  $\mathbf{y}$  is an output vector,  $\mathbf{A}, \mathbf{B}, \mathbf{G}$  are matrices that define the dynamic system and  $\mathbf{C}, \mathbf{D}$  are matrices that describe the output from sensors, where  $\mathbf{D}$  is generally set to zero and  $\mathbf{C}$  is an identity matrix if all states are measured by sensors.

### 2.1 Aircraft State Space Models

For fixed-wing aircraft, the linearized state space model comes from Taylor expanding the aircraft kinematic and dynamic equations of motion about an equilibrium (or trim) condition. Because this derivation is well documented in the literature (see Stevens 2016, Beard 2012, or Schmidt 2012), it will not be reiterated in this paper. It suffices to say that the nonlinear aircraft equations of motion

are derived from kinematics, rigid-body dynamics, and the aerodynamic, propulsive, and gravitational forces and moments on the aircraft.

Fixed-wing aircraft dynamics can be decomposed into lateral and longitudinal models, where lateral refers to roll, heading, and side-to-side motion and longitudinal refers to pitch, vertical, and forward motion. For most fixed-wing airframes, the coupling between these two directions is small (Beard 2012). The wind velocity state observer used in this work uses reduced order lateral and longitudinal models, which are described by the following states and inputs:

$$\mathbf{x}_{lat} = [v \ p \ r \ \phi]^T \quad \mathbf{x}_{lon} = [u \ w \ q \ \theta]^T \quad (2.2a)$$

$$\mathbf{u}_{lat} = [\delta_a \ \delta_r]^T \quad \mathbf{u}_{lon} = [\delta_e \ \delta_t]^T \quad (2.2b)$$

where  $u, v, w$  represent the inertial aircraft translational velocities projected onto the aircraft body frame of reference (see Fig. 1),  $\phi, \theta, \psi$  are the aircraft attitude angles: roll, pitch, and yaw (also called Euler angles), and  $p, q, r$  are the angular rates with respect to the aircraft body frame. The inputs,  $\delta_e, \delta_a, \delta_r$  are the elevator, aileron, and rudder deflections, respectively, and  $\delta_t$  is the throttle percentage from maximum. Each of these terms has the trim value subtracted from it.

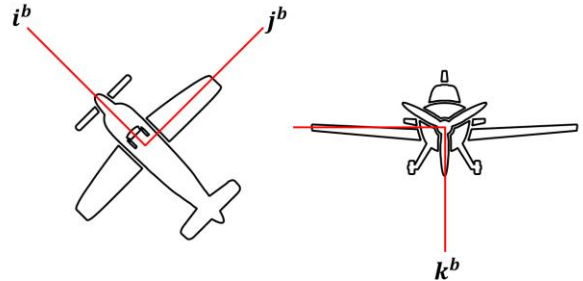


FIG. 1. Aircraft body frame of reference.

### 2.2 Wind Velocity States

In simulations of aircraft motion, the wind velocity enters in through  $\mathbf{d}$ ,

$$\mathbf{d}_{lat} = [v_d \ p_d \ r_d]^T \quad \mathbf{d}_{lon} = [u_d \ w_d \ q_d]^T \quad (2.3)$$

Where  $u_d, v_d, w_d$  is the inertial translational wind velocity in aircraft body coordinates and  $p_d, q_d, r_d$  are three components of the wind velocity gradient tensor projected in the aircraft body frame which will be referred to as angular wind velocity hereafter,

$$p_d = \frac{\partial w_d}{\partial y} \quad q_d = \frac{\partial w_d}{\partial x} \quad r_d = \frac{\partial v_d}{\partial x} \quad (2.4)$$

This vector is often generated through a turbulence model, such as the Dryden Turbulence Model, and given as an additional input into the aircraft system. In order to estimate the wind velocity through a *state* observer, however, it is necessary to represent  $\mathbf{d}$  as a state in the system. This is most easily accomplished by representing  $\mathbf{d}$  in a state space model and augmenting the wind velocity states onto  $\mathbf{x}$ . The total wind velocity vector can be represented by,

$$\mathbf{d} = \mathbf{d}_s + \mathbf{d}_g \quad (2.5)$$

where  $\mathbf{d}_s$  represents a steady ambient wind and  $\mathbf{d}_g$  is a stochastic wind component or “gust” that can be modeled by passing white noise through a shaping filter. To illustrate this, say that the total wind velocity can be represented in the following manner,

$$\dot{\mathbf{x}}_s = 0 \quad (2.6a)$$

$$\dot{\mathbf{x}}_g = \mathbf{A}_g \mathbf{x}_g + \mathbf{B}_g \mathbf{n} \quad (2.6b)$$

$$\mathbf{d} = \mathbf{x}_s + \mathbf{C}_g \mathbf{x}_g \quad (2.6c)$$

Then, one can augment Eqn. 2.1a with wind velocity “states” like so,

$$\begin{bmatrix} \dot{\mathbf{x}} \\ \dot{\mathbf{x}}_g \\ \dot{\mathbf{x}}_s \end{bmatrix} = \begin{bmatrix} \mathbf{A} & \mathbf{G}\mathbf{C}_g & \mathbf{G} \\ \mathbf{0} & \mathbf{A}_g & \mathbf{0} \\ \mathbf{0} & \mathbf{0} & \mathbf{0} \end{bmatrix} \begin{bmatrix} \mathbf{x} \\ \mathbf{x}_g \\ \mathbf{x}_s \end{bmatrix} + \begin{bmatrix} \mathbf{B} \\ \mathbf{0} \\ \mathbf{0} \end{bmatrix} \mathbf{u} + \begin{bmatrix} \mathbf{0} \\ \mathbf{B}_g \\ \mathbf{0} \end{bmatrix} \mathbf{n} \quad (2.7a)$$

$$\tilde{\mathbf{y}} = \begin{bmatrix} \mathbf{C} \\ \mathbf{0} \\ \mathbf{0} \end{bmatrix} \begin{bmatrix} \mathbf{x} \\ \mathbf{x}_g \\ \mathbf{x}_s \end{bmatrix} \quad (2.7b)$$

For ease, this will furthermore be represented as,

$$\dot{\tilde{\mathbf{x}}} = \tilde{\mathbf{A}}\tilde{\mathbf{x}} + \tilde{\mathbf{B}}\mathbf{u} + \tilde{\mathbf{B}}_g \mathbf{n} \quad (2.8a)$$

$$\tilde{\mathbf{y}} = \tilde{\mathbf{C}}\tilde{\mathbf{x}} \quad (2.8b)$$

By incorporating the wind term in this fashion, the wind states  $\mathbf{x}_s$  and  $\mathbf{x}_g$  can be estimated through a state observer.

### 2.3 Wind Velocity State Observer

The state observer works by reducing the error between an estimated state vector,  $\hat{\mathbf{x}}$ , and the

actual state vector exponentially in time. By creating an estimated state equation of the form,

$$\dot{\hat{\mathbf{x}}} = (\tilde{\mathbf{A}} - \mathbf{L}\tilde{\mathbf{C}})\hat{\mathbf{x}} + (\tilde{\mathbf{B}} - \mathbf{L}\tilde{\mathbf{D}})\mathbf{u} + \mathbf{L}\tilde{\mathbf{y}} \quad (2.9)$$

the rate of change of the error between  $\tilde{\mathbf{x}}$  and  $\hat{\mathbf{x}}$  is

$$\begin{aligned} \dot{\mathbf{e}} &= \dot{\tilde{\mathbf{x}}} - \dot{\hat{\mathbf{x}}} \\ &= (\tilde{\mathbf{A}} - \mathbf{L}\tilde{\mathbf{C}})\mathbf{e} + \tilde{\mathbf{B}}_g \mathbf{n} \end{aligned} \quad (2.10)$$

By assuming that the noise,  $\mathbf{n}$ , is white noise and has a mean of zero, then observer gain,  $\mathbf{L}$ , can be optimally chosen through a Riccati equation such that the error is minimized to a steady state value. In this study, the value of  $\mathbf{L}$  was selected using MATLAB’s function, `kalman`.

In this form, the state observer is able to make wind velocity estimates without acceleration feedback, but the information contained in accelerations provides significant improvement in error when fed back through the observer.

### 2.4 Acceleration Feedback

The acceleration terms come in through the output vector,  $\tilde{\mathbf{y}}$ , by appending the rate of change of the aircraft states,  $\dot{\mathbf{x}}$ , to the other known sensor measurements,

$$\tilde{\mathbf{y}}_{accel} = \begin{bmatrix} \mathbf{C}\mathbf{x} \\ \dot{\mathbf{x}} \end{bmatrix} = \begin{bmatrix} \mathbf{C}\mathbf{x} \\ \mathbf{A}\mathbf{x} + \mathbf{B}\mathbf{u} + \mathbf{G}\mathbf{d} \end{bmatrix} \quad (2.11)$$

Expressed in terms of  $\tilde{\mathbf{x}}$ , this equation becomes,

$$\tilde{\mathbf{y}}_{accel} = \begin{bmatrix} \mathbf{C} & \mathbf{0} & \mathbf{0} \\ \mathbf{A} & \mathbf{G}\mathbf{C}_g & \mathbf{G} \\ \mathbf{0} & \mathbf{0} & \mathbf{0} \end{bmatrix} \begin{bmatrix} \mathbf{x} \\ \mathbf{x}_g \\ \mathbf{x}_s \end{bmatrix} + \begin{bmatrix} \mathbf{0} \\ \mathbf{B} \\ \mathbf{0} \end{bmatrix} \mathbf{u} \quad (2.12)$$

Replacing this value for  $\tilde{\mathbf{y}}$  in the estimated state dynamics shown in Eqn. 2.9 ultimately improves the wind velocity estimates because of the additional state information being provided from sensors.

In order to obtain the rate of change of the aircraft states from distributed accelerometers, it is necessary to understand the relationship between the two. Gremillion et al. (2016) showed that an accelerometer can be considered a point along a rigid body. The total acceleration of the point is

$$\begin{aligned} \mathbf{a}_{P/O} &= \mathbf{a}_{O/O} + \mathbf{a}_{P/O'} + \boldsymbol{\alpha} \times \mathbf{r}_{P/O'} + 2\boldsymbol{\omega} \times \mathbf{v}_{P/O'} \\ &\quad + \boldsymbol{\omega} \times (\boldsymbol{\omega} \times \mathbf{r}_{P/O'}) \end{aligned} \quad (2.13)$$

where  $O$  represents the origin of a fixed coordinate frame,  $O'$  represents the center of gravity (CG) of a moving rigid body, and  $P$  represents a point on the rigid body, such that  $r_{O'/O}$  refers to the distance between the two coordinate frames and  $r_{P/O'}$  refers to the distance between a point on the rigid body and the CG (see Fig. 2). The first two terms represent the translational acceleration, followed by Euler, Coriolis, and centripetal acceleration terms, respectively.

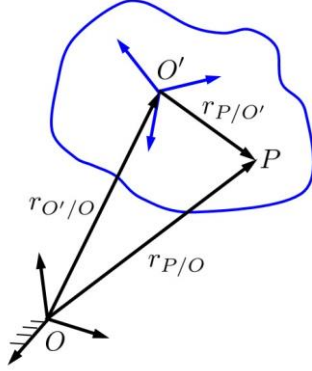


FIG. 2. Diagram of a coordinate frame of a moving rigid body. Gremillion 2016.

When this equation is expressed in body coordinates, the point on the body does not move with respect to the body's coordinate axes, thus the second and fourth terms reduce to zero. This simplifies the equation to:

$$\mathbf{a}_{P/O} = \mathbf{a}_{O'/O} + \boldsymbol{\alpha} \times \mathbf{r}_{P/O'} + \boldsymbol{\omega} \times (\boldsymbol{\omega} \times \mathbf{r}_{P/O'}) \quad (2.14)$$

Let  $\mathbf{r}_{P/O'}$  represent the position vector from the CG of an sUAS to a uniaxial accelerometer. This can be denoted by:

$$\mathbf{r}_i = [x_i \ y_i \ z_i]^T \quad (2.15)$$

where the subscript represents the  $i$ th accelerometer and the position coordinates are given in the aircraft body frame of reference. In a similar manner, let  $\mathbf{a}_{P/O}$  be designated by  $\mathbf{a}_i$ , which refers to the total inertial acceleration of the accelerometer projected onto body coordinates. Eqn. 2.14 can then be written in terms of the aircraft angular rates and accelerations as,

$$\mathbf{a}_i = \begin{bmatrix} a_x - (q^2 + r^2)x_i + (pq - \dot{r})y_i + (pr + \dot{q})z_i \\ a_y + (pq + \dot{r})x_i - (p^2 + r^2)y_i + (qr - \dot{p})z_i \\ a_z + (pr - \dot{q})x_i + (qr + \dot{p})y_i - (q^2 + p^2)z_i \end{bmatrix} \quad (2.16)$$

The actual output of the accelerometer,  $\eta_i$ , is related to this acceleration by

$$\eta_i = \kappa_i \hat{\mathbf{e}}_i^T \mathbf{a}_i + b_i \quad (2.17)$$

where  $\kappa_i$  is a sensitivity gain term,  $b_i$  is the accelerometer bias and  $\hat{\mathbf{e}}_i^T$  is the orientation of the accelerometer. The orientation refers to the projection of body frame accelerations onto the sensitivity axes of the accelerometer.

By defining an acceleration state vector,  $\mathbf{x}_a$ , such that

$$\mathbf{x}_a = [a_x \ a_y \ a_z \ \dot{p} \ \dot{q} \ \dot{r} \ p^2 \ q^2 \ r^2 \ pq \ pr \ qr]^T \quad (2.18)$$

where  $\mathbf{a}_{cg} = [a_x \ a_y \ a_z]$  represents the translational acceleration of the aircraft projected into body coordinates,  $\dot{p}, \dot{q}, \dot{r}$  are angular accelerations, and the rest are cross terms that are unused in the state observer, the accelerometer output can be rewritten as,

$$\boldsymbol{\eta} = \begin{bmatrix} \eta_1 \\ \eta_2 \\ \cdot \\ \cdot \\ \eta_n \end{bmatrix} = \mathbf{C}_a \mathbf{x}_a + \mathbf{b} \quad (2.19)$$

where  $\mathbf{C}_a$  is a matrix comprised of the sensitivity gain and orientation of each accelerometer. Rearranging this equation and taking the pseudo-inverse yields a relationship between the acceleration state vector and the accelerometer output,

$$\mathbf{x}_a = (\mathbf{C}_a^T \mathbf{C}_a)^{-1} \mathbf{C}_a (\boldsymbol{\eta} - \mathbf{b}) \quad (2.20)$$

Because  $(\mathbf{C}_a^T \mathbf{C}_a)$  must be invertible and  $\mathbf{x}_a$  has 12 components, the minimum number of uniaxial accelerometers is  $n \geq 12$ , which is equivalent to 4 tri-axial accelerometers.

The acceleration state vector requires a few additional steps before it can be used in the state observer. First, the inertial accelerations  $a_x, a_y, a_z$  are not equivalent to  $\dot{u}, \dot{v}, \dot{w}$  because they are vector

derivatives taken in two different frames of reference. The relationship between the two is:

$$\begin{aligned}\dot{u} &= a_x + rv - qw \\ \dot{v} &= a_y + pw - ru \\ \dot{w} &= a_z + qu - pv\end{aligned}\quad (2.21)$$

Second, the Euler rates are not related to the acceleration state vector, but can be found from angular rate information through the following transformation:

$$\begin{bmatrix} \dot{\phi} \\ \dot{\theta} \\ \dot{\psi} \end{bmatrix} = \begin{bmatrix} 1 & \sin(\phi)\tan(\theta) & \cos(\phi)\tan(\theta) \\ 0 & \cos(\phi) & -\sin(\phi) \\ 0 & \sin(\phi)\sec(\theta) & \cos(\phi)\sec(\theta) \end{bmatrix} \begin{bmatrix} p \\ q \\ r \end{bmatrix}\quad (2.22)$$

In order to obtain all of the aircraft state rates of change for use in the state observer, it is assumed that the aircraft is equipped with gyros to determine  $p, q, r$  and GPS to determine  $u, v, w$ .

### 3. SIMULATION SETUP

This section describes a simulation of lateral and longitudinal wind velocity observers that were developed in MATLAB and Simulink. The observers were implemented on lateral and longitudinal aircraft models of the Twistor UAS that were buffeted by simulated wind velocities for 30 seconds using a 0.001 time step. The control inputs were simulated through linear quadratic regulator (LQR) feedback control to keep the aircraft as close to straight and level as possible. It was assumed that all of the aircraft states and aircraft state rates of change ( $x$  and  $\dot{x}$ ) were known perfectly, that there was no ambient wind ( $x_g = 0$ ), and that the aircraft dynamics were perfectly modeled through a linear state space representation.

The simulation was conducted in two separate parts:

- 1) The Twistor was simulated using the dynamics shown in Eqn. 2.1a and buffeted by simulated wind. This produced “true” aircraft states, controls, and accelerations that were fed into the wind velocity observer.
- 2) The observer was tested using the estimated state dynamics shown in Eqn. 2.9

These steps are more clearly depicted in Fig. 3.

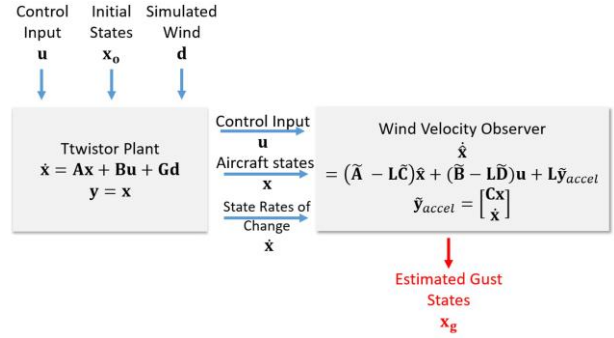


FIG. 3. Diagram of simulation setup.

### 3.1 Twistor Specifications

The Twistor is a fixed-wing sUAS with twin engine propellers on each wing that provide thrust, a T-shaped tail with a rudder for yawing motion, and elevators and ailerons on the wings for pitch and roll (see Fig. 4). The mass, speed, and geometry of this aircraft are provided in Table 3.1.



FIG. 4. Twistor UAS in flight. (University of Colorado Boulder 2017)

	Symbol	Value	Units
Mass	$m$	5.74	kg
Wingspan	$b$	3.22 m	m
Wing Area	$S$	0.6282	m <sup>2</sup>
Mean Chord	$c$	0.2080	m
Inertia	$I_{xx}$	1.20	kg m <sup>2</sup>
	$I_{yy}$	0.932	
	$I_{zz}$	2.0734	
	$I_{xz}$	0.0946	

TABLE 5. Twistor mass and geometric properties.

This platform was chosen for simulation primarily due to the availability of lateral and longitudinal state space models. The aircraft stability derivatives, engine parameters, drag terms, and moments of inertia were produced by Roadman et al. (2012). These parameters were used in Maio et al. (2018) to compute the aerodynamic coefficients that make up the  $A, B,$

and  $\mathbf{G}$  matrices used in Eqn. 2.1a. The linear model parameters were calculated assuming average flight conditions in Boulder, CO using density values from the International Standard Atmosphere (ISA) model.

Recall that the linear model assumes the states are perturbations from a trim condition. The trim conditions were obtained by minimizing the Ttwistor's nonlinear aerodynamic force and moment equations. The non-zero trim conditions are given in Table 3.2.

Trim State	Value	Units
$h^*$	-1800	m
$V_a^*$	18	m/s
$\theta^*$	0.0515	rad
$u^*$	17.976	m/s
$w^*$	0.9263	m/s

Trim Input	Value	Units
de	-0.537	rad
dt	0.1792	(frac)

TABLE 2. Ttwistor trim states and control inputs.

### 3.2 Simulated Control Inputs

The control inputs were designed using standard LQR feedback control, such that

$$\mathbf{u} = -\mathbf{K}\mathbf{x} \quad (3.1)$$

where  $\mathbf{K}$  is the optimal matrix that forces aircraft states to the trim condition in a very similar manner to the Kalman Filter selection of  $\mathbf{L}$ . The feedback system was designed in MATLAB using the `lqr` command. To make the simulation more realistic, the surface deflections were limited by upper and lower saturation values of  $\pm 45^\circ$  and the throttle was bounded from 0 to 1. The resulting control inputs throughout the simulation are shown in Fig. 5.

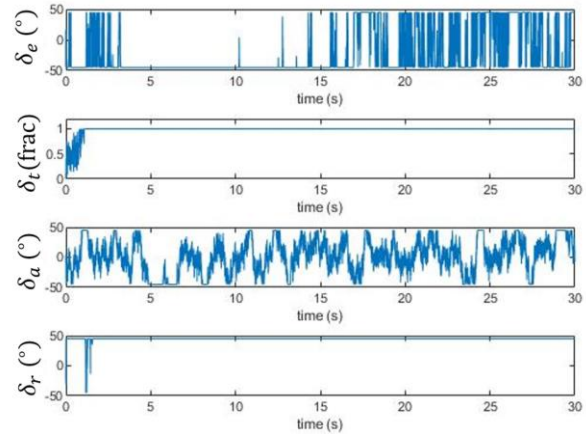


FIG. 6. Simulated control inputs: elevator deflection, thrust limit, aileron deflection, and rudder deflection.

### 3.3 Simulated Wind Velocities

The Ttwistor was buffeted by simulated wind produced from three different Simulink blocks: the continuous Dryden Wind Turbulence, Discrete Gust, and Wind Shear blocks. Fig. 6 shows how this was set up. The turbulence length scale was set to 533.4 m and the turbulence intensity was set to 0.1944 for an altitude of 1800 m mean sea level (MSL) within the Dryden Turbulence Block. The Dryden Turbulence model was also used to define the  $\mathbf{A}_g$ ,  $\mathbf{B}_g$ , and  $\mathbf{C}_g$  matrices shown in Eqns. 2.6b and 2.6c. The Discrete Gust block was given a magnitude of 1 m/s in all translational body axes and the Shear Wind block was given a magnitude of 3 m/s coming from  $20^\circ$  clockwise from north. The resulting simulated wind velocities with discrete and shear terms are shown in Fig. 7.

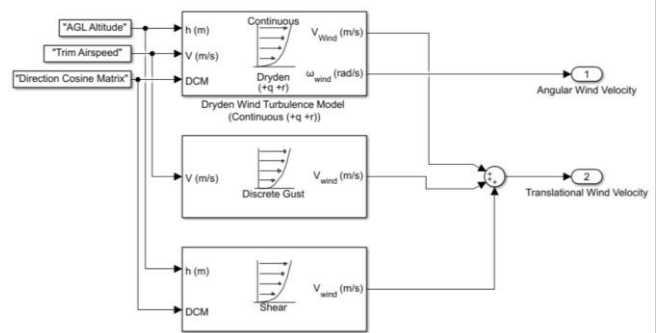
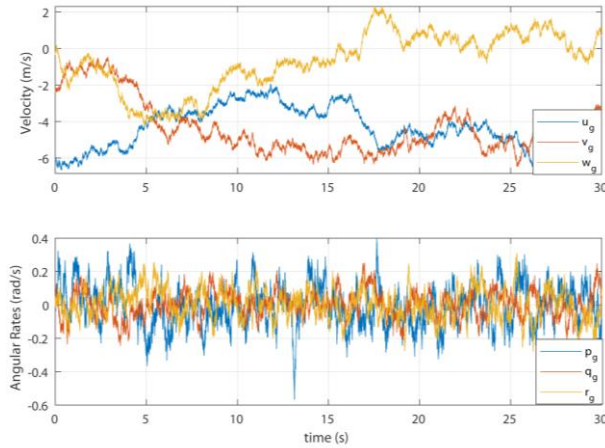


FIG. 7. Simulink Diagram for three gust types: Dryden model gusts, discrete gusts, and wind shear.



**FIG. 8.** Translational and angular simulated gusts in body frame coordinates.

### 3.4 Sensor Model

Band limited white noise was applied to the states and rates of change that were subsequently fed into the wind velocity observer. These states primarily correspond to GPS, accelerometer, and gyro measurements. The noise power was computed using the noise PSD values located on the InvenSense MPU-6050 data sheet (InvenSense 2018). The data sheet lists a noise PSD of  $0.005 \text{ }^\circ/\text{s}/\sqrt{\text{Hz}}$  for the gyros and  $400 \text{ } \mu\text{g}/\text{s}/\sqrt{\text{Hz}}$  for the accelerometers.

### 3.5 Observer Setup

The lateral and longitudinal wind velocity observers were simulated using the dynamic model given in Eqn. 2.9. The  $\tilde{A}$  and  $\tilde{B}$  matrices were obtained from the aircraft and wind models described in the previous sections. All of the control inputs, aircraft states, and aircraft state rates of change used in the observer were produced from simulating the aircraft in windy conditions. Initial conditions for the estimated aircraft states and control inputs were chosen arbitrarily in order to show convergence to the correct wind velocities. The simulation was run both with and without feedback from the aircraft state rates of change that are associated with distributed accelerometer measurement. This was done to show the improvements in wind velocity estimation when using acceleration terms in the observer.

## 3.6 Diagrams of Simulation

The following diagrams show the simulation of the Twistor and subsequent inputs to the wind velocity observer in more detail:

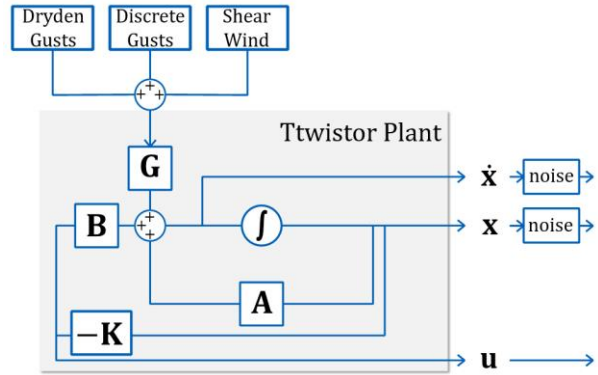


**FIG. 9.** Diagram of Twistor simulation. The aircraft was buffeted with three types of wind. Control inputs were simulated to stabilize the aircraft. The resulting outputs were fed into the wind velocity observer.

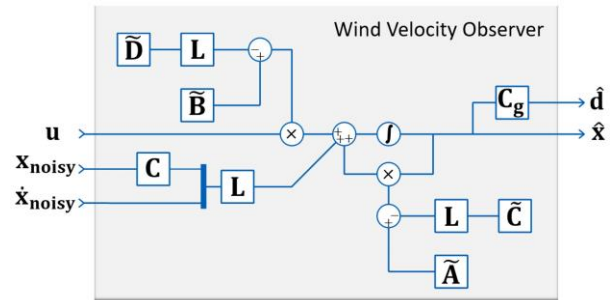


**FIG. 10.** Diagram of the wind velocity observer. Inputs, states, and state rates of change were given from the aircraft simulation. The resulting outputs are the estimated wind velocities and aircraft states.

## 4. RESULTS

The wind velocity estimates from the observer show convergence to the correct wind velocity values regardless of incorrect initial conditions both with and without acceleration feedback. However, the error from the wind velocity estimates is significantly lower when using acceleration terms in the observer feedback than without these terms. The following plots show the lateral and longitudinal wind velocity estimates as compared to the actual simulated velocities and the estimated wind velocities without acceleration feedback.

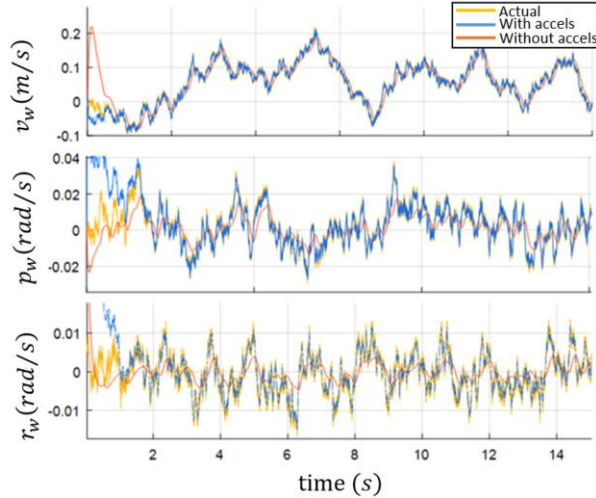


**FIG. 11.** Lateral wind velocity estimates. The wind velocity observer with acceleration feedback (blue) is compared to the actual states (yellow) and the observer without acceleration feedback (red).

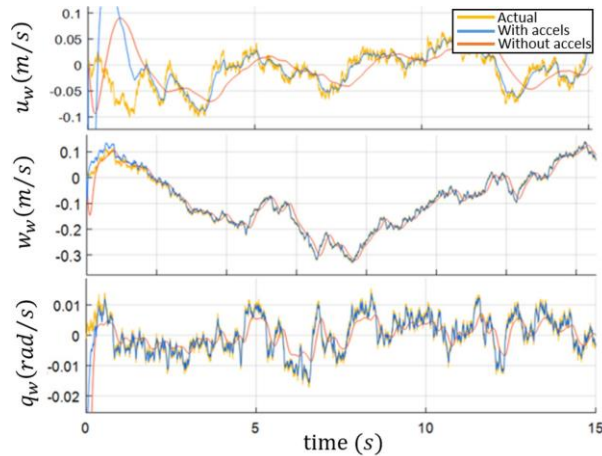


**FIG. 12.** Longitudinal wind velocity estimates. The wind velocity observer with acceleration feedback (blue) is compared to the actual states (yellow) and the observer without acceleration feedback (red).

These plots show that the observer produces wind velocity estimates that converge to the correct values both with and without acceleration feedback. With acceleration feedback, the error of the wind velocity estimates is significantly reduced. This is further emphasized in the following histogram of errors.

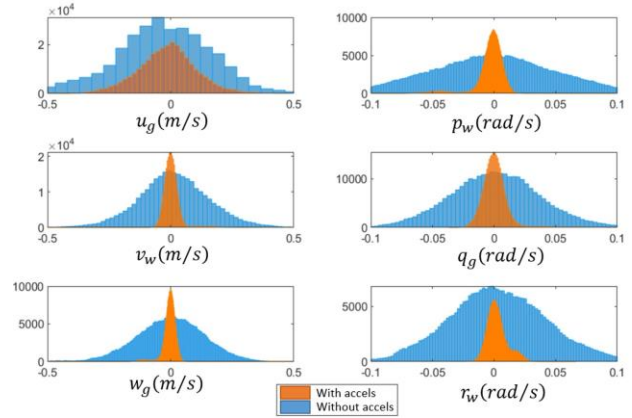


**FIG. 13.** Histogram of errors for wind velocity observer with (orange) and without (blue) acceleration feedback.

The following table shows the standard deviation of the errors for both sets of wind velocity estimates. From this, one can see an obvious improvement in the observer with the use of acceleration feedback.

	Standard Deviation	
	With Accels	Without Accels
$u_g$ (m/s)	0.0979	0.2212
$v_g$ (m/s)	0.0237	0.1204
$w_g$ (m/s)	0.0179	0.1415
$p_g$ (rad/s)	0.0062	0.0525
$q_g$ (rad/s)	0.0074	0.0374
$r_g$ (rad/s)	0.0060	0.0402

**TABLE 3.** Standard deviation of errors for wind velocity observer with and without acceleration feedback.

## 5. CONCLUSION

Standard methods of wind velocity measurement are prohibitively expensive in terms of size, weight, power, and cost for use on sUAS. This paper describes a method of wind velocity estimation that does not rely on any airspeed measurements, but rather utilizes lightweight and cheap aircraft sensors such as GPS and IMUs. The addition of translational and angular accelerations in the observer feedback via a distributed acceleration sensor suite can greatly improve wind velocity estimates. This was shown with simulation using a Ttwistor UAS platform that was buffeted by simulated wind gusts and wind shear. The results showed a viable method of wind estimation that is within 1 m/s for translational wind velocity

estimation and within 0.1 rad/s for angular wind velocity estimation.

Future work includes using the wind velocity observer with experimental data from flight using a fixed-wing UAS equipped with a distributed accelerometer sensor suite, GPS, and an IMU. The resulting wind velocity estimates will be compared to relative wind data from an onboard multi-hole probe that is transformed into inertial wind using GPS information. The observer will then be implemented onboard for real-time wind velocity estimates during experimental flight.

## ACKNOWLEDGEMENTS

The first author would like to acknowledge the Center for Unmanned Aircraft Systems (CUAS) and the National Science Foundation for providing the funding for this research under Grant No. 1650468.

## REFERENCES

- Aeroprobe, 2018. Micro ADC models. [Available online at <http://www.aeroprobe.com/micro-air-data-computer-models>].
- Avery, A. and J. Jacob, 2015. Design of a severe storm research UAS. In 53rd AIAA Aerospace Sciences Meeting. AIAA. doi: 10.2514/6.2015-1905.
- Beard, R.W. and T. W. McClain, 2012. Small Unmanned Aircraft: Theory and Practice. Princeton University Press.
- Cho, A., J. Kim, S. Lee, C. Kee, 2011. Wind estimation and airspeed calibration using a UAV with a single-antenna GPS receiver and pitot tube. IEEE Transactions on Aerospace and Electronic Systems, 47:109-117, doi: 10.1109/TAES.2011.5705663.
- Cybyk, B.Z., B. McGrath, T.M. Frey, D.G. Drewry, J.F. Keane, G. Patnaik, 2009. Unsteady urban air flows and their impact on small unmanned air system operations. In AIAA Atmospheric Flight Mechanics Conference. AIAA. doi: 10.2514/1.1010000.
- Gremillion, G.M. and J.S. Humbert, 2016. Disturbance rejection with distributed acceleration sensing for small unmanned aircraft systems. AIAA Journal, 54:2233-2246. doi:10.2514/1.J054408.
- InvenSense, 2018. Mpu-6000 and mpu-6050 product specification revision 3.4. [Available online at <https://www.invensense.com/wp-content/uploads/2015/02/MPU-6000-Datasheet1.pdf>].
- Johansen, T.A., A. Cristofaro, K. Sorensen, J. M. Hansen, T.I. Fossen, 2015. On estimation of wind velocity, angle-of-attack and sideslip angle of small UAVs using standard sensors. In International Conference on Unmanned Aircraft Systems. IEEE. doi: 10.1109/ICUAS.2015.7152330.
- Maio, A., B. Ranganathan, J. S. Humbert, G. Gremillion, W. Nothwang, 2018. Acceleration feedback control for fixed-wing sUAS. In IEEE Aerospace Conference. IEEE. doi: 10.1109/AERO.2018.8396639.
- Pisano, W. and D. Lawrence, 2009. Control limitations of small unmanned aerial vehicles in turbulent environments. In AIAA Guidance, Navigation, and Control Conference. AIAA, 2009. doi:10.2514/6.2009-5909.
- Quindlen, J. and J. Langelaan, 2013. Flush air data sensing for soaring-capable UAVs. In 51<sup>st</sup> AIAA Aerospace Sciences Meeting. AIAA. doi: 10.2514/6.2013-1153.
- Reuder, J., M.O. Jonassen, H. Olafsson, 2012. The small unmanned meteorological observer SUMO: Recent developments and applications of a micro-uas for atmospheric boundary layer research. Acta Geophys, 60:1454-1473, doi: 10.2478/s11600-012-0042-8.
- Roadman, J.R., J. Elston, B. Argrow, E.W. Frew, 2012. Mission performance of the tempest UAS in supercell storms. AIAA Journal of Aircraft, 49:1821- 1830. doi: 10.2514/1.C031655.
- Schmidt, D.K, 2012. Modern Flight Dynamics. McGraw-Hill.
- Stevens, B.L, F.L. Lewis, E.N. Johnson, 2016. Aircraft Control and Simulation. Wiley.
- Weibel. D., 2015. Improving the Accuracy of in-situ lower ABL wind measurements using sUAS. PhD thesis, University of Colorado at Boulder.